Research Article

Wei Wang, Bo Zhang, Lanhua Cui, Hongwei Zheng, Jiří Jaromír Klemeš, and Jin Wang*

Numerical study on heat transfer and flow characteristics of nanofluids in a circular tube with trapezoid ribs

https://doi.org/10.1515/phys-2021-0022
received October 25, 2020; accepted March 03, 2021

Abstract: This study aims to investigate heat transfer and flow characteristics of ethylene glycol/water (EGW) and CuO–EGW nanofluids in circular tubes with and without trapezoid ribs. Nusselt number and friction factor in tubes with trapezoid ribs are analysed under a constant heat flux by changing rib bottom angles. This study compares the convective heat transfer coefficients of 6 vol.% CuO–EGW nanofluid and base fluid. It is found that under a constant Reynolds number, the Nusselt number and friction factor for CuO–EGW nanofluid and base fluid increase with an increase in the inclination angle. The Nusselt number for the CuO–EGW nanofluid in the tube with 75° rib bottom angle averagely increases by 135.8% compared to that in the smooth tube, and the performance evaluation criterion is 1.64.

Keywords: nanofluids, trapezoid rib, heat transfer enhancement, angle, friction factor

*** Corresponding author: Jin Wang,** School of Energy and Environmental Engineering, Hebei University of Technology, Tianjin 300401, China; Sustainable Process Integration Laboratory – SPIL, NETME Centre, Faculty of Mechanical Engineering, Brno University of Technology – VUT Brno, Technická 2896/2, 616 69 Brno, Czech Republic, e-mail: wjwcn00@163.com
Wei Wang: Innovation and Entrepreneurial Center, Hebei University of Technology, Tianjin 300401, China
Bo Zhang: School of Energy and Environmental Engineering, Hebei University of Technology, Tianjin 300401, China
Lanhua Cui: Library, Hebei University of Technology, Tianjin 300401, China
Hongwei Zheng: Experimental Training Center, Hebei University of Technology, Tianjin 300401, China
Jiří Jaromír Klemeš: Sustainable Process Integration Laboratory – SPIL, NETME Centre, Faculty of Mechanical Engineering, Brno University of Technology – VUT Brno, Technická 2896/2, 616 69 Brno, Czech Republic

Nomenclature

u_i	axial velocity (m s^{-1})
u_j	radial velocity (m s^{-1})
u'	fluctuated velocity (m s^{-1})
q	Wall heat flux (W m^{-2})
T	temperature (K)
f	friction factor, dimensionless
Nu	Nusselt number, dimensionless
Re	Reynolds number, dimensionless
Pr	Prandtl number, dimensionless
ΔP	pressure drop (Pa)
k	turbulent kinetic energy (J kg^{-1})
u	mean flow velocity (m s^{-1})
$\dot{m}$	mass flow rate (kg s^{-1})
PEC	performance evaluation criteria
h	convective heat transfer coefficient (W m^{-2} K^{-1})
$S_{\mathrm{gen,T}}$	total entropy generation rate (W K^{-1})
$S_{\mathrm{gen,h}}$	thermal entropy generation rate (W K^{-1})
$S_{\mathrm{gen,f}}$	friction entropy generation rate (W K^{-1})
L	length of tube (m)
D_{S}	the outer diameter of tube (m)
D_{f}	the inner diameter of tube (m)
D	hydraulic diameter (m)

Greek letters

ρ	density (kg m^3)
μ	dynamic viscosity (kg m^{-1} s^{-1})
ε	turbulence dissipation rate (m^3 s^{-2})
c_{p}	specific heat capacity (J kg^{-1} K^{-1})
λ	thermal conductivity (W m^{-1} K^{-1})

1 Introduction

Heat exchangers have numerously been applied to the industrial field, such as air conditioning, power station,

chemical industry and so on. Rib structures have been studied to enhance the heat transfer performance of heat exchangers in recent years. Al-Jethelah et al. [1] conducted a numerical study about the melting process of phase-change materials in a rectangular thermal storage unit. Results showed that the Nusselt number (Nu) and melt fraction were significantly affected at the beginning of convective heat transfer coefficient and melting rate. Mohammed et al. [2] numerically examined the effects of three different structural parameters for circular tubes with transverse corrugation (rib pitch-to-tube diameter, rib height-to-tube diameter and rib width-to-tube diameter) on the thermal performance of water. It was reported that friction factor increased with an increase in corrugation height. In six-start spirally corrugated pipes, Jin et al. [3] carried out a numerical study on flow resistance characteristics of the tubes with various geometric parameters (such as pitch and depth). Results showed that they had 1.28–3.45 times the resistance coefficient of the circular tube when Reynolds number ranged from 100 to 1,000. Jiang et al. [4] developed a two-dimensional heat transfer model for a tube filled with porous medium inserts. Results showed that in comparison with that for the smooth tube, the heat transfer coefficient for the tube with the porous media is enhanced 6–7.76 times. Hærvig et al. [5] numerically investigated heat transfer characteristics in 28 different corrugated tubes by changing the geometrical parameters. Results showed that the recirculation zone disappeared by increasing the corrugation length. In the helically coiled tube, Zhang et al. [6] numerically studied heat transfer characteristics of the tube with spherical corrugation. Results revealed that the heat transfer performance for the tube with spherical corrugation was enhanced 1.05–1.7 times compared with the smooth tube. Sun and Zeng [7] numerically investigated the heat transfer performance inside a corrugated tube with three structural parameters. Results showed that in comparison with that of plain tubes, the heat transfer performance of the corrugated tube was enhanced by 50%. Youcef and Saim [8] conducted numerical investigations of turbulent flow dynamics and heat transfer enhancement in heat exchanger with a shell and tube. It was found that compared with the shell and tube heat exchanger without baffles, the case with baffles had 1.86 and 21.67% increases in the heat transfer coefficient and the pressure drop. Xin et al. [9] investigated the heat transfer and flow characteristics of oscillatory flow in a two-start spirally corrugated tube. The simulated results indicated that the heat transfer enhancement of the corrugated tube is 1.38 times compared to that of the smooth tube.

Several studies about the heat transfer performance of the tube filling with nanofluids have recently confirmed the improvement in the heat transfer efficiency by using numerical and experimental methods. For CuO–, Al_2O_3– and SiO_2–ethylene glycol/water (EGW) nanofluids, Namburu et al. [10] numerically analysed the heat transfer characteristics of these nanofluids flowing through a circular tube under a constant heat flux. It was observed that the heat coefficient of the CuO–EGW nanofluid with the volume concentration of 6% increased by 1.75 times than that of the EG/water. Kristiawan et al. [11] investigated the heat transfer characteristics of TiO_2/water with the volume concentration of 1.18% flowing inside a circular tube by using innovative numerical method. Results showed that the heat transfer was increased by 21.87% compared to the water. Feizabadi et al. [12] numerically investigated the heat transfer characteristics of Al_2O_3/water in a twisted-serpentine tube with empirical validation. Results detected that the Nu for the twisted-serpentine tube with a straight length of 0.10 m, the serpentine pitch of 0.03 m and twisted pitch of 0.05 m increased by 35% compared to the twisted-straight tube. In a helically coiled tube, Omidi et al. [13] numerically investigated the heat transfer applications of the tubes with different lobed cross sections. Results showed that the heat transfer for Al_2O_3/water in the tube with a lobed number of 6 increased by 28% compared to that for the water. For TiO_2–H_2O nanofluids in tubes with different corrugation pitches, Wang et al. [14] experimentally investigated heat transfer performance and resistance coefficient. Results showed that the heat transfer performance of the corrugated tubes was improved by 4.8–66.3% compared with the water under the same working conditions. Mei et al. [15] experimentally analysed heat transfer characteristics of Fe_3O_4–water nanofluids in the corrugated and smooth tubes. Results indicated that the Nu for the Fe_3O_4–water nanofluids in the corrugated tube increased by 35.8% compared to that in the smooth tube. Zhai et al. [16] experimentally investigated heat transfer and flow characteristics of TiO_2–water nanofluids in spiral tubes. Results found that for the 0.5% TiO_2–water nanofluid, the heat transfer efficiency of the spiral tube with a 100-mm screw pitch increased by 55.7% compared to that of the horizontal tube. Kristiawan et al. [17] experimentally investigated the friction factor and thermal performance of a tube with helical micro-fins using TiO_2/water nanofluid. Results indicated that thermal performance of 0.30 vol.% TiO_2/water nanofluid was increased by 51% compared to the water.

From the previous publications, it is found that few studies discussed the effect of the ribs. In this study, a turbulent behaviour of CuO–EGW nanofluid in a circular

tube will be investigated in detail. Moreover, heat transfer and friction factors of both the CuO–EGW nanofluid and the EGW fluid will be analysed by considering the effect of the different trapezoid ribs.

2 Mathematical modelling

Three-dimensional models with various trapezoid ribs are designed to study heat transfer characteristics of the CuO–EGW nanofluid.

2.1 Physical modelling and assumptions

Figure 1 shows the schematic diagram of the tube with the trapezoid ribs. In the computational domain, the length (L), the outer (D_s) and inner diameters (D_f) of the tube are 800, 12 and 10 mm, respectively.

The structure of the smooth tube and the tubes with the periodic rib configuration with the various angles of 15–75° is illustrated in Figure 2. The spacing between the ribs is 20 mm, and the inlet and outlet sections are of the same value of 30 mm. The smooth case 1 represents a tube without a rib angle. The tubes with different rib angles are named as cases 2–6. For the trapezoid ribs with the same height of 2.5 mm, the long side is a fixed value of 20 mm in the x direction, whereas the short side in the x direction is depended upon the inclination angles.

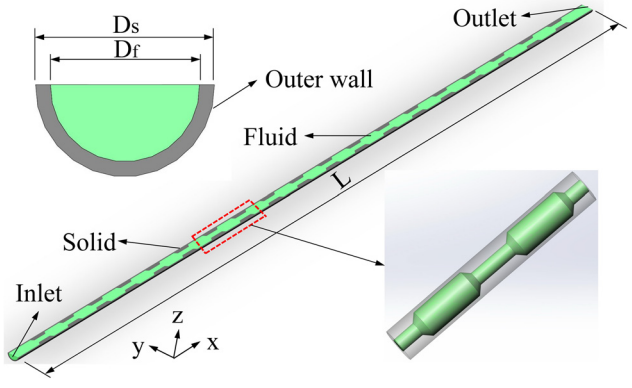

Figure 1: Tube structure with trapezoid ribs.

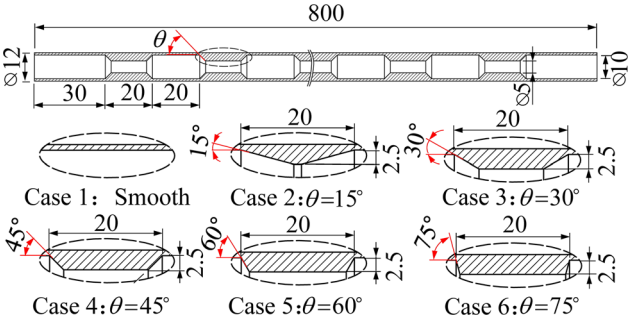

Figure 2: Rib structures with different angles (unit: mm).

2.2 Governing equations

In the related physical phenomenon, the governing equations are listed as follows:

Continuity equation:

$$\frac{\partial(\rho u_i)}{\partial x_i} = 0 \tag{1}$$

Momentum equation:

$$\begin{aligned}&\frac{\partial}{\partial t}(\rho u_i) + \frac{\partial}{\partial x_j}(\rho u_i u_j)\\ &= -\frac{\partial P}{\partial x_i} + \frac{\partial}{\partial x_j}\left[\mu\left(\frac{\partial u_i}{\partial x_j} + \frac{\partial u_j}{\partial x_i} - \frac{2}{3}\delta_{ij}\frac{\partial u_j}{\partial x_j}\right)\right]\\ &\quad + \frac{\partial}{\partial x_j}(-\rho\overline{u'_j u'_j})\end{aligned} \tag{2}$$

Energy equation:

$$\begin{aligned}&\frac{\partial}{\partial t}(u_i(\rho E + P))\\ &= \frac{\partial}{\partial x_i}\left[\left(\lambda + \frac{c_p u_t}{Pr_t}\right)\frac{\partial T}{\partial x_j} + \mu u_i\left(\frac{\partial u_i}{\partial x_j} + \frac{\partial u_j}{\partial x_i} - \frac{2}{3}\delta_{ij}\frac{\partial u_j}{\partial x_j}\right)\right]\end{aligned} \tag{3}$$

where the ρ, μ, u_i, u_j, u', c_p and λ are density of fluid, dynamic viscosity, axial velocity, radial velocity, fluctuated velocity, specific heat capacity and thermal conductivity, respectively. The E is the total energy as follows:

$$E = c_p T - \frac{P}{\rho} + \frac{u^2}{2} \tag{4}$$

The turbulent stresses and heat flux quantities were expressed by using the realizable k–ε turbulent model [18]. The addition equations were shown in the present numerical simulation.

The turbulent kinetic energy (k) equation:

$$\frac{\partial}{\partial x_i}(\rho k u_i) = \frac{\partial}{\partial x_i}\left[\left(\mu + \frac{\mu_t}{\sigma_k}\right)\frac{\partial k}{\partial x_j}\right] + G_k - \varepsilon \tag{5}$$

The rate of dissipation (ε) equation:

$$\frac{\partial}{\partial x_i}(\varepsilon u_i) = \frac{\partial}{\partial x_i}\left[\left(\mu + \frac{\mu_t}{\sigma_\varepsilon}\right)\frac{\partial \varepsilon}{\partial x_i}\right] + C_1 \varepsilon G_k - C_2\left(\frac{\varepsilon^2}{k + \sqrt{v\varepsilon}}\right) \quad (6)$$

where

$$G_k = -\overline{u_i u_j}\frac{\partial u_i}{\partial u_j} = \mu_t\left(\frac{\partial u_i}{\partial x_j} + \frac{\partial u_j}{\partial x_i}\right)\frac{\partial u_i}{\partial x_i} \quad (7)$$

The σ_k and σ_ε are the effective Prandtl numbers for turbulent kinetic energy and the rate of dissipation, respectively. C_1 and C_2 are constants.

Eddy viscosity μ_t is given by equation:

$$\mu_t = (\rho C_\mu k^2)/\varepsilon \quad (C_\mu = 0.09) \quad (8)$$

Empirical constants for the turbulence model are offered by Launder and Spalding [19].

$C_1 = 1.44$; $C_2 = 1.92$; $\sigma_k = 1.0$; $\sigma_\varepsilon = 1.3$.

2.3 Data acquisition

The Nu is calculated by:

$$\mathrm{Nu} = hD/\lambda \quad (9)$$

where h and D are the convective heat transfer coefficient and the hydraulic diameter.

Friction factor is calculated by:

$$f = \frac{2\Delta P D}{\rho u^2 L} \quad (10)$$

where ΔP and u are the pressure drop and the mean flow velocity of the whole tube, respectively.

The total entropy generation can be expressed from Bejan et al. [20], Moghaddami et al. [21] and Bianco et al. [22] as follows:

$$S_{\mathrm{gen,T}} = S_{\mathrm{gen,h}} + S_{\mathrm{gen,f}} = \frac{q^2 \pi D^2 L}{Nu\lambda T^2} + \frac{32\dot{m}^3 f}{\pi^2 \rho^2 T D^5} \quad (11)$$

where $S_{\mathrm{gen,T}}$ stands for total entropy generation rate, $S_{\mathrm{gen,h}}$ and $S_{\mathrm{gen,f}}$ are entropy generation rates due to heat transfer and fluid friction. T, q and $\dot{m}$ are the temperature of nanofluid, the wall heat flux and mass flow rate, respectively. ρ and λ are the density and the thermal conductivity of the nanofluid, respectively. D and L are diameter and length of the tube, respectively.

In order to investigate the heat transfer surfaces of the tube with the periodic rib configuration, the performance evaluation criterion (PEC) was defined by Gee and Webb [23] and Li et al. [24] as follows:

$$\mathrm{PEC} = \frac{\mathrm{Nu_t}/\mathrm{Nu_s}}{(f_t/f_s)^{1/3}} \quad (12)$$

where $\mathrm{Nu_t}$ and $\mathrm{Nu_s}$ stand for Nu of the ribbed tube and the smooth tube, respectively. f_t and f_s are the friction factor of the ribbed tube and the smooth tube, respectively.

2.4 Thermal properties

In order to analyse the heat transfer characteristics of the CuO–EGW nanofluid, all thermophysical properties at a temperature of 293 K are illustrated in Table 1 [10].

2.5 Boundary conditions

In the inlet section, the fluid velocity is assumed uniform, and the fluid temperature is a fixed value of 293 K. The inner wall/fluid contact surface is set as the coupled wall. The inlet wall and outlet wall at solid domain are adiabatic. An outflow boundary condition is applied to the outlet. The outer wall for the tube is assumed to have a uniform heat flux q of 5×10^5 W/m^2. In the present numerical analysis, the enhanced wall treatment is applied to the near wall.

2.6 Numerical method

Numerical simulations are performed by using the commercial software ANSYS Fluent 18.0 [25]. The semi-implicit

Table 1: Thermophysical properties of the nanofluid and EGW at 293 K in the present work

Fluid	Volume concentration (%)	Density (kg/m^3)	Specific heat (J/kg K)	Thermal conductivity (W/m K)	Viscosity (mPa s)
EGW	0	1,086	3,084	0.349	5.380
CuO–EGW	6	1,411	2,379	0.412	19.360

method for pressure-linked equation (SIMPLE) was chosen to couple the velocity field with the pressure field. The discretisation scheme of the finite volume method was carried out in the computation domain by following the first-order upwind for both momentum and energy equations. For continuity, the residuals of x–y–z velocities, κ and ε, were lower than 10^{-6}. The residual for energy was lower than 10^{-10}, and all the solutions in the present work are assumed to be converged.

2.7 Grid independence study

Non-uniform structured grids are used for the tubes with trapezoid ribs, as shown in Figure 3. A grid refinement is conducted near the interface between the solid and fluid domains. Boundary layer meshes at the adjacent wall of near-wall regions were used to meet the requirement of $y^+ < 1$. Several different mesh sizes were used for the grid independence test. At Reynolds number of 20,000, compared with the Nu from case 4 with 2.310 M grids, the cases with 0.820, 1.268 and 1.565 M grids show the deviations of 5.20, 3.31 and 1.06%, respectively. The friction factor of the cases with 0.820, 1.268 and 1.565 M grids shows the deviations of 5.17, 3.92 and 1.21% compared with 2.310 M grids, respectively. Finally, the cases with above 1.565 M grids were used for the present research.

3 Results and discussion

This part will discuss the effects of structure parameters (six circular tubes with trapezoid ribs) using EGW fluid and CuO–EGW nanofluid.

3.1 Validation of the present simulation

In order to validate the numerical model, Nu and friction factors for CuO–EGW nanofluid from the present study are compared with the calculated results by Namburu et al. [10], Gnielinski correlation [26] and Blasius formula [27] as follows:

$$\mathrm{Nu} = 0.012(\mathrm{Re}^{0.87} - 280)\mathrm{Pr}^{0.4},\ 1.5 \le \mathrm{Pr} \le 500,\quad 3 \times 10^3 \le \mathrm{Pr} \le 10^6. \tag{13}$$

$$f = 4C_\mathrm{f} = 4(0.0791\mathrm{Re}^{-1/4}) \tag{14}$$

The average Nu and friction factor (f) for EGW and CuO–EGW nanofluids with 6% volume concentration are used for the working fluid in a smooth tube at Reynolds number of 20,000. Comparisons of the Nu and f are shown in Figures 4 and 5.

For the EGW in Figure 4, the average errors of Nu and f between the simulated results from Namburu et al. [10] and the results calculated in the present study are 4.4 and 1.6%. The average error of Nu between the results of the Gnielinski correlations and the results of the present study is 7.2%. On the other hand, compared with the results calculated by the Blasius formula and the present

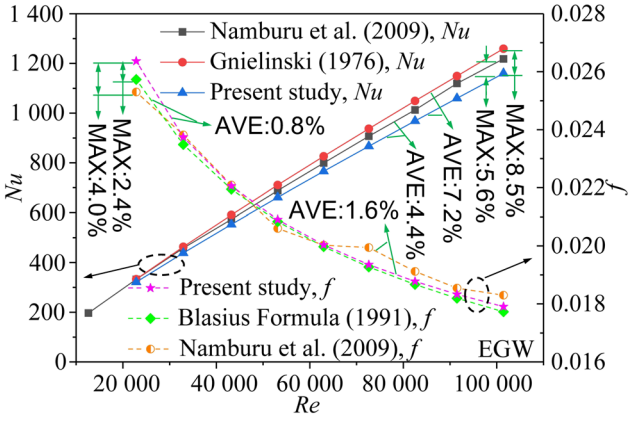

Figure 4: Nu and f for the EGW in the smooth tube.

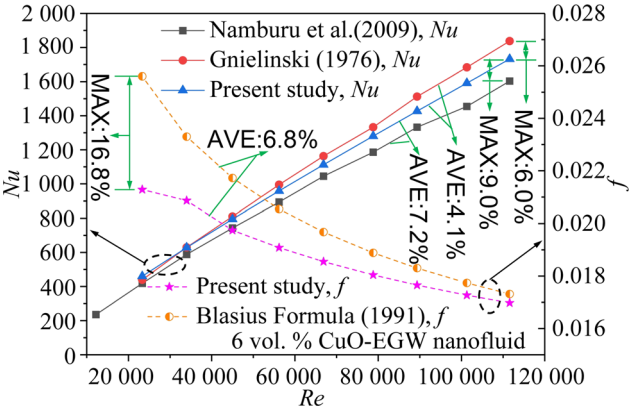

Figure 5: Nu and f for the CuO–EGW nanofluid in the smooth tube.

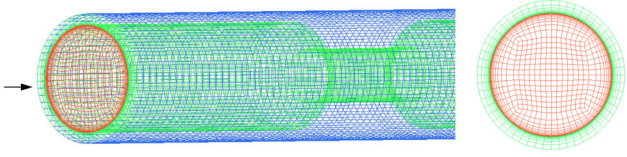

Figure 3: Computational grids of a tube with trapezoid ribs.

work, the average error of f is 0.8%. For the CuO–EGW nanofluid, the average errors of Nu and f are presented in Figure 5. The average error of Nu between the results simulated by Namburu et al. [10] and the present research is 7.2%, whereas the average error of Nu between the results of the Gnielinski correlation and the current research is 4.1%. Compared with the results of Blasius formula and the present research, the maximum and average errors of f are 16.8 and 6.8%, respectively. These results indicate that the present study about the EGW and CuO–EGW nanofluid shows a good agreement with the previous publications.

3.2 Effects of the rib angles for the EGW

Figures 6 and 7 show the Nu and f of the EGW at Reynolds number of 20,000–100,000 in six different tubes. From Figure 6a, it is found that Nu increases linearly with an increase in the Reynolds number. The EGW in the tube with the trapezoid ribs shows larger Nu than that in the smooth tube, due to the presence of secondary flow and the increase in the heat transfer surface. For the same Reynolds number, it is understood that the Nu of the EGW increases with the increase in the rib bottom angle of the tube as shown in Figure 6a. This is caused by the boundary layer near the wall that is intensively interrupted by the trapezoid rib with high bottom angles, which enhances the heat transfer in the tubes. A vortex is formed when the EGW flows through the tubes with the trapezoid ribs. This process has strengthened the mixing of fluid, which makes thermal boundary more thinker compared to the smooth tube. Compared to the smooth tube, the average Nu incremental values for the tubes with the rib angles of 15°, 30°, 45°, 60° and 75° are 57.1, 96.0, 108.1, 123.0 and 131.2%, respectively (Figure 7a).

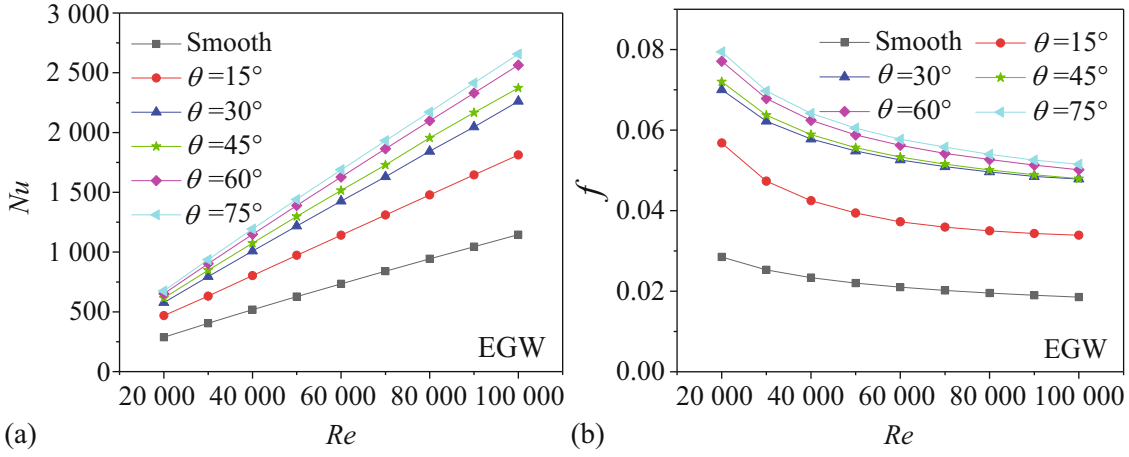

Figure 6: Heat transfer and flow characteristics of the EGW in tubes with different trapezoid ribs: (a) variations in Nu with Re, (b) variations in f with Re.

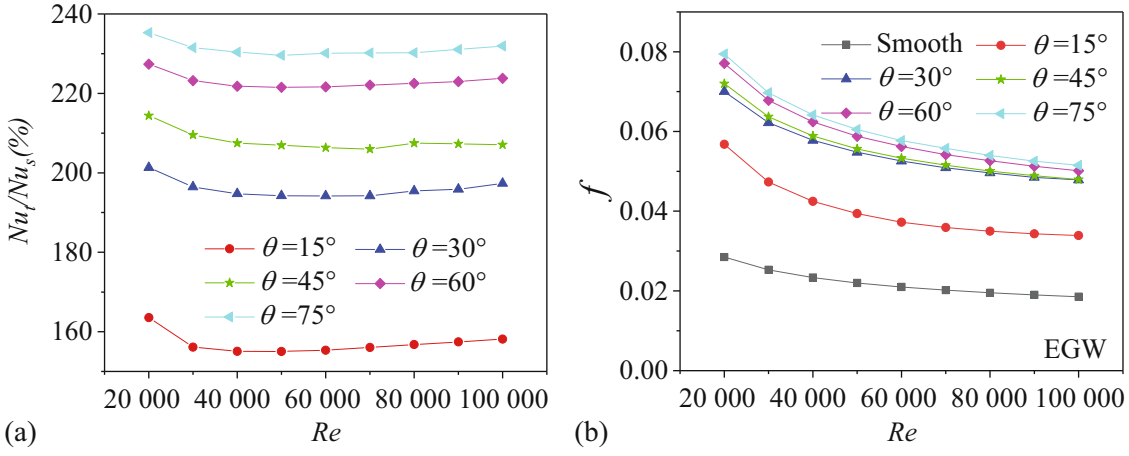

Figure 7: Comparisons of Nu and f of the EGW between tubes with different trapezoid ribs and the smooth tube: (a) variations in Nu_t/Nu_s with Re, (b) variations in f_t/f_s with Re.

In Figure 6b, it is illustrated that the f gradually decreases with the increase in the Reynolds number in the smooth tube. In comparison with the smooth tube, the f in all the tubes with the trapezoid ribs increases as expected due to the addition of the ribs in the inner wall. The f for all the tubes with the trapezoid ribs increases with the increase in the rib angles at the same Reynolds number. As shown in Figure 7b, compared to the smooth tube, the f values of the tubes with the rib angles of 15°, 30°, 45°, 60° and 75° increase by 82.8, 150.9, 154.5, 168.8 and 176.2%, respectively.

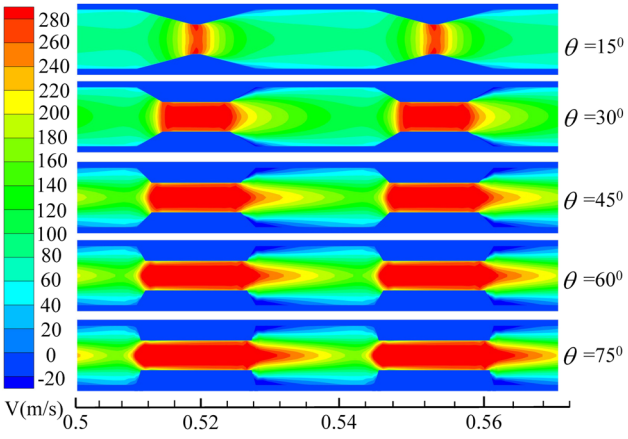

Figure 8: Velocity distribution in tubes with trapezoid ribs at Re of 50,000.

3.3 Effects of the rib angles for the CuO–EGW nanofluid

As shown in Figure 8, the velocity distribution diagrams of the tubes with different trapezoid ribs are obtained by numerical simulation. It is found that for a tube, the velocity of medium at the part with trapezoid ribs is higher than that at the part without trapezoid ribs. This phenomenon is due to the sudden shrinkage of the flow area caused by the trapezoid ribs. The process of inter-switcher between flow acceleration and deceleration promotes the formation of vortexes, which is beneficial to the increase in turbulence to interrupt the boundary layer. With the increase in bottom angles, the period of the inter-switcher becomes shorter, and vortices will be generated in the mutation section. Therefore, the trapezoid rib with a larger bottom angle has a greater potential to enhance the heat transfer.

Figure 9a shows the Nu incremental ratios of the CuO–EGW nanofluid by comparison with those of the EGW in the same working condition.

It is found that the CuO–EGW nanofluid has higher thermal conductivity compared to the EGW in the same tube due to the destruction of the boundary layer from nanoparticles. The intense Brownian motion of nanoparticles in the CuO–EGW nanofluid can destroy the boundary layer, which reduces the thermal resistance between the nanofluid and the innerwall. For all the tubes with the trapezoid ribs, the maximum incremental ratio of the Nu for the CuO–EGW nanofluid occurred

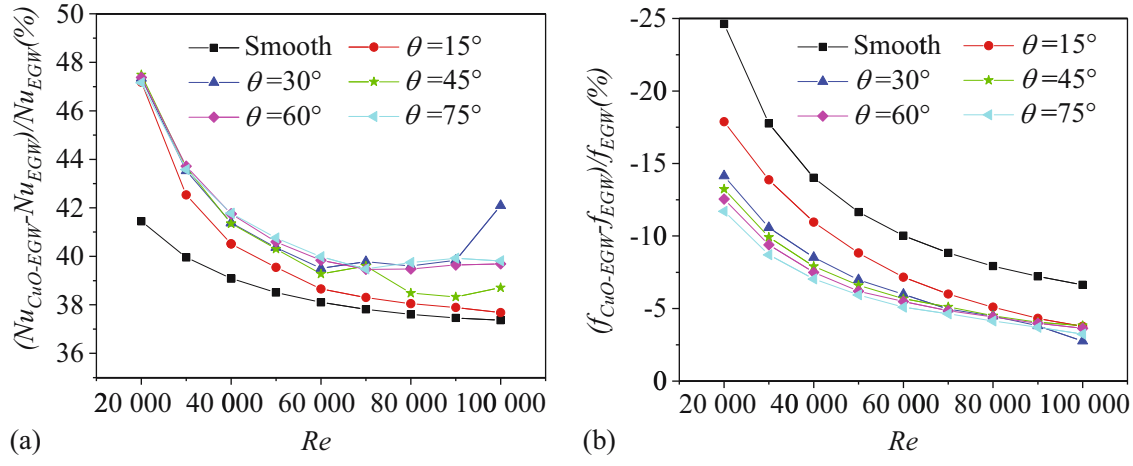

Figure 9: Comparisons of Nu and f between the EGW and CuO–EGW nanofluid: (a) Nu incremental ratios with Re (b) f incremental ratios with Re.

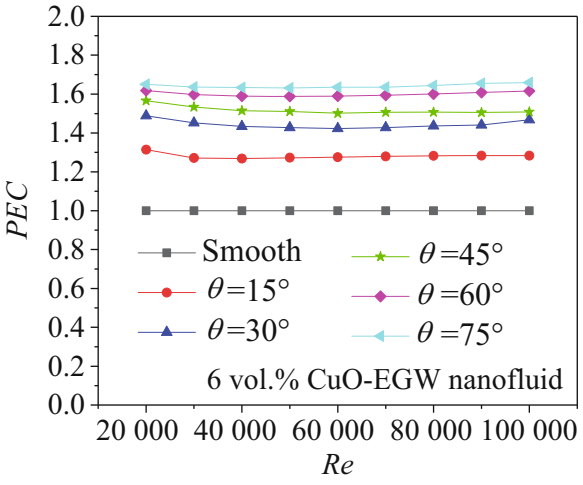

Figure 10: Variations in PEC for the CuO–EGW nanofluid with Re.

at Reynolds number of 20,000 compared to the EGW. In addition, as the Reynolds number increases in the range of 20,000–60,000, the incremental ratio rapidly decreases. The Nu for the CuO–EGW in the tubes with the rib angles of 60° and 75° significantly decreases first and then increases. The Nu for the CuO–EGW in the tubes with trapezoid ribs of the angle of 30° and 45° has a small fluctuation at the Reynolds number of 60,000–100,000. For the CuO–EGW nanofluid in a smooth tube, the Nu for the CuO–EGW nanofluid increases by 38.6% on average compared to the EGW. Compared with the EGW in the tubes with the rib angles of 15°, 30°, 45°, 60° and 75°, the average Nu values for the CuO–EGW nanofluid increase by 40.0, 41.5, 40.8, 41.2 and 41.3%. The CuO–EGW nanofluid in the tubes with the rib angles of 15°–75° shows average Nu increases of 58.7, 100.0, 111.4, 127.3 and 135.8% compared to the smooth tube.

As shown in Figure 9b, in comparison with the EGW, the f of the CuO–EGW nanofluid in the smooth tube averagely decreases by 12.1%, and the f of the CuO–EGW nanofluid in the tubes with the rib angles of 15°–75° averagely decreases by 8.6, 6.9, 6.8, 6.4 and 6.0%. In addition, the f values in the tubes with the rib angles of 15°–75° averagely increase by 90.2, 166.0, 170.5, 186.7 and 196.0% compared to that in the smooth tube.

From Figure 10, it is observed that the PEC is higher than 1 at Reynolds number of 20,000–100,000. The

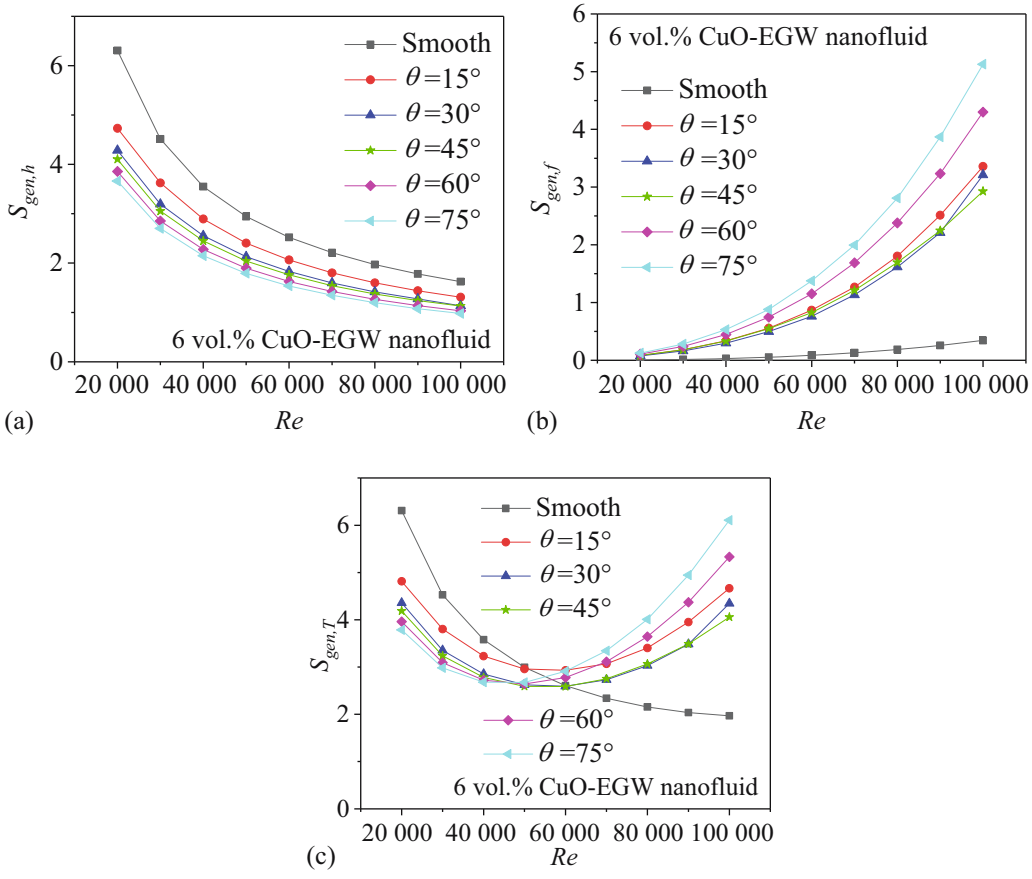

Figure 11: Effects of different trapezoid ribs on $S_{gen,h}$, $S_{gen,f}$ and $S_{gen,T}$: (a) variations in $S_{gen,h}$ with Re, (b) variations in $S_{gen,f}$ with Re, (c) variations in $S_{gen,T}$ with Re.

results indicate that the performance of the tube with trapezoid ribs is better than the smooth tube. The maximum value of PEC appears for the trapezoid ribs with the 75° bottom angle, and the average value is 1.64.

3.4 Effects of the rib angles for the CuO–EGW nanofluid on entropy generation rate

Figure 11 shows the effects of different trapezoid ribs in the tube on $S_{gen,h}$, $S_{gen,f}$ and $S_{gen,T}$ with Reynolds number.

Figure 11a shows that the $S_{gen,h}$ decreases with the increase in the Reynolds number in six tubes and the reduction in the bottom angles of the trapezoid ribs. The tubes with the trapezoid ribs result in lower $S_{gen,h}$ values compared to the smooth tube at the same Reynolds number. In Figure 11b, it is observed that the $S_{gen,f}$ increases with the increase in the Reynolds number and the bottom angles in trapezoid ribs. The tube with the trapezoid ribs leads to higher $S_{gen,f}$ compared to the smooth tube. As shown in Figure 11c, it is found that with the increase in the Reynolds number in the tubes with trapezoid ribs, the $S_{gen,T}$ first decreases and then increases. The increase in the Reynolds number causes a decreasing trend of $S_{gen,T}$ due to the dominance of $S_{gen,h}$. The increase in the bottom angles affects the growth of $S_{gen,f}$, which leads to a reduction in $S_{gen,h}$. When the balance point between $S_{gen,h}$ and $S_{gen,f}$ is reached, the optimal condition will be obtained. The balance point for the tubes with trapezoid ribs appears at Reynolds number of 50,000. At Reynolds number of 20,000–50,000, the trapezoid ribs with 75° bottom angle show better performance (due to smaller total entropy generation) compared to other ribs.

4 Conclusion

This study numerically investigated the heat transfer performances in the smooth tube filled with EGW and the CuO–EGW nanofluid. In addition, the Nu and friction factor (f) for the EGW and the CuO–EGW nanofluid in the tubes with the rib angles of 15°–75° are also analysed. The main conclusions are drawn as follows:

(1) For the EGW in the tubes with various rib angles, a better heat transfer performance is obtained compared with that in the smooth tube. The EGW with the rib angle of 75° shows the maximum incremental Nu value, and the Nu increases by 131.2% compared with the smooth tube.
(2) The Nu for the CuO–EGW nanofluid showed a significant increase compared to the EGW, whereas the f for the CuO–EGW nanofluid showed a significant reduction. The Nu for the CuO–EGW nanofluid averagely increases by 41.5% for the tube with 45° rib angle compared to the EGW, whereas the f for the CuO–EGW nanofluid averagely decreases by 6.9%.
(3) For the CuO–EGW nanofluid, the Nu in the tubes with ribs are higher than the value in the smooth tube. The tube with the rib angle of 75° shows the maximum incremental ratio of the Nu values between the tubes with and without ribs, and the average value is 135.8%, whereas the value is 1.64 in PEC.

Acknowledgement: This study was supported by the National Natural Science Foundation of Hebei Province of China (Grant Number E2019202184) and the Project of Innovation Ability Training for Postgraduate Students of Education Department of Hebei Province under Grant (Grant Number CXZZSS2019012). The authors acknowledge the funding and support by the EU project Sustainable Process Integration Laboratory – SPIL, project no. CZ.02.1.01/0.0/0.0/15_003/0000456, by Czech Republic Operational Programme Research and Development, Education, Priority 1: Strengthening capacity for quality research operated by the Czech Ministry of Education, Youth and Sport.

Conflict of interest: Authors state no conflict of interest.

References

[1] Al-Jethelah M, Al-Sammarraie A, Tasnim S, Mahmud S, Dutta A. Effect of convection heat transfer on thermal energy storage unit. Open Phys. 2018;16:861–7.
[2] Mohammed HA, Abbas AK, Sheriff JM. Influence of geometrical parameters and forced convective heat transfer in transversely corrugated circular tubes. Int Commun Heat Mass Transf. 2013;44:116–26.
[3] Jin ZJ, Liu BZ, Chen FQ, Gao ZX, Gao XF, Qian JY. CFD analysis on flow resistance characteristics of six-start spirally corrugated tube. Int J Heat Mass Transf. 2016;103:1189–207.
[4] Jiang YG, Feng Y, Zhang SL, Qin J, Bao W. Numerical heat transfer analysis of transcritical hydrocarbon fuel flow in a tube partially filled with porous media. Open Phys. 2016;14:659–67.
[5] Hærvig J, Sørensen K, Condra TJ. On the fully-developed heat transfer enhancing flow field in sinusoidally, spirally

corrugated tubes using computational fluid dynamics. Int J Heat Mass Transf. 2017;106:1051–62.
[6] Zhang CC, Wang DB, Xiang S, Han Y, Peng X. Numerical investigation of heat transfer and pressure drop in helically coiled tube with spherical corrugation. Int J Heat Mass Transf. 2017;113:332–41.
[7] Sun M, Zeng M. Investigation on turbulent flow and heat transfer characteristics and technical economy of corrugated tube. Appl Therm Eng. 2018;129:1–11.
[8] Youcef A, Saim R. Comparative numerical study of turbulent forced convection in a shell and tube heat exchanger between the simple case and with cross baffles. Chem Eng Trans. 2018;71:955–60.
[9] Xin F, Liu ZC, Zhen NB, Liu P, Liu W. Numerical study on flow characteristics and heat transfer enhancement of oscillatory flow in a spirally corrugated tube. Int J Heat Mass Transf. 2018;127:402–13.
[10] Namburu PK, Das DK, Tanguturi KM, Vajjha RS. Numerical study of turbulent flow and heat transfer characteristics of nanofluids considering variable properties. Int J Therm Sci. 2009;48:290–302.
[11] Kristiawan B, Santoso B, Wijayanta AT, Aziz M, Miyazaki T. Heat transfer enhancement of TiO_2/water nanofluid at laminar and turbulent flows: a numerical approach for evaluating the effect of nanoparticle loadings. Energies. 2018;11:1584.
[12] Feizabadi A, Khoshvaght-Aliabadi M, Rahimi, AB. Numerical investigation on Al_2O_3/water nanofluids flow through twisted-serpentine tube with empirical validation. Appl Therm Eng. 2018;137:296–309.
[13] Omidi M, Farhadi M, Darzi AAR. Numerical strudy of heat transfer on using lobed cross sections in helical coil heat exchangers: Effect of physical and geometrical parameters. Energy Convers Manage. 2018;176:236–45.
[14] Wang GZ, Qi C, Liu MN, Li CY, Yan YY, Liang L. Effect of corrugation pitch on thermo-hydrauli performance of nanofluids in corrugated tubes of heat exchanger system based on exergy efficiency. Energy Convers Manage. 2019;186:51–65.
[15] Mei SY, Qi C, Luo T, Zhai XF, Yan YY. Effects of magnetic field on therm-hydraulic performance of Fe_3O_4-water nanofluids in a corrugated tube. Int J Heat Mass Transf. 2019;128:24–45.
[16] Zhai XF, Qi C, Pan YH, Luo T, Liang L. Effects of screw pitches and rotation angles on flow and heat transfer characteristics of nanofluids in spiral tubes. Int J Heat Mass Transf. 2019;130:989–1003.
[17] Kristiawan B, Rifa'I AI, Enoki K, Wijayanta AT, Miyazaki T. Enhancing the thermal performance of TiO_2/water nanofluids flowing in a helical microfins tube. Powder Technol. 2020;356:254–62.
[18] El Maakoul A, Laknizi, A, Saadeddine S, El Metoui M, Zaite A, et al. Numerical comparison of shell-side performance for shell and tube heat exchangers with trefoil-hole, helical and segmental baffles. Appl Therm Eng. 2016;109:175–85.
[19] Launder BE, Spalding DB. The numerical computation of turbulent flows. Comput Methods Appl Mech Eng. 1974;3:269–89.
[20] Bejan A. Enropy generation minimization. Boca Raton: CRC Press; 1996.
[21] Moghaddami M, Mohammadzade A, Esfehani S. Second law analysis of nanofluid flow. Energy Convers Manage. 2011;52:1397–405.
[22] Bianco V, Manca O, Nardini S. Performance analysis of turbulent convection heat transfer of Al_2O_3 water-nanofluid in circular tubes at constant wall temperature. Energy. 2014;77:403–13.
[23] Gee DL, Webb RL. Forced convection heat transfer in helically rib-roughened tubes. Int J Heat Mass Transf. 1980;23:1127–36.
[24] Li M, Khan TS, Hajri EA, Ayub ZH. Geometric optimization for thermal–hydraulic performance of dimpled enhanced tubes for single phase flow. Appl Therm Eng. 2016;103:639–50.
[25] ANSYS Inc. ANSYS fluent 18.0 users guide, fluent documentation. New York, USA: ANSYS Inc; 2017.
[26] Gnielinski V. New equations for heat and mass transfer in turbulent pipe and channel flow. Int Chem Eng. 1976;16:187–91.
[27] White FM. Viscous fluid flow. New York, USA: McGraw Hill; 1991.